

# Signatures of general gravitational waves in cosmic microwave background

Jun Li<sup>1,2,\*</sup>

<sup>1</sup>*School of Mathematics and Physics, Qingdao University of Science and Technology, Qingdao 266061, China*

<sup>2</sup>*CAS Key Laboratory of Theoretical Physics, Institute of Theoretical Physics,  
Chinese Academy of Sciences, Beijing 100190, China*

(Dated: March 22, 2022)

We investigate the signatures of general gravitational waves in cosmic microwave background (CMB) by extending the state of the universe. The equation of state influences the evolution of gravitational waves owing to the damping rate. The tensor perturbations generate anisotropies and polarization which show signatures in the tensor power spectra. We consider how general gravitational waves affect CMB power spectra and explore the constraints on the cosmological parameters in general states  $\omega = \{0, 1/9, 1/4, 1/3, 2/3, 1\}$  from Planck+BK15+BAO datasets. In the  $\Lambda$ CDM+ $r$  model, the impacts on the tensor-to-scalar ratio are obvious. We also measure the tensor power spectra parameters in general states from gravitational waves observations within LIGO, LISA, IPTA, FAST and SKA projects, respectively.

## I. INTRODUCTION

Inflation assumes that in the early universe a small patch underwent a period of rapid exponential expansion which became the universe we observe today [1]. The observed universe looks so homogeneous and isotropic on large scales because inhomogeneities were wiped out. The inflationary expansion comes from quantum fields and stretches these perturbations from microphysical to cosmological scales. The small fluctuations of inflation field are related to fluctuations of the metric. The metric perturbations contain scalar perturbations and tensor perturbations which generate density perturbations and gravitational waves [2–7]. These perturbations reenter the observable universe after inflation and generate anisotropies and polarization which have been confirmed by the cosmic microwave background (CMB). CMB is a probe to explore the early universe and the cosmological evolution.

Most studies of cosmological perturbations concentrate on the evolution in radiation domination or matter domination. However, the whole evolution of early universe is a long variational process, the state of the universe need enough time to alter which could not change from kinetic domination to radiation domination or from radiation domination to matter domination suddenly. Some recent papers focus on variational states, such as the quantum chromodynamic (QCD) phase transition provide a definitive equation of state of the universe [8], the equation of state is parameterized by thermodynamics variables [9]. The equation of general states have been used to explore the scalar induced gravitational waves [9, 10]. The state of the universe also influences the gravitational waves propagation. Furthermore, the evolution of gravitational waves can be affected by three ways: the damping rate of gravitational waves, the dispersion relation and an addi-

tional source term on the perfect fluid. We have explored the signatures of modified dispersion relation of graviton in CMB [11]. See more related references from [12–23].

In this paper, we investigate the signatures of general gravitational waves in CMB by extending the state of the universe. When we consider general states of the universe, the equations and behaviors of gravitational waves change according to parameter  $\omega$  which influences the damping rate of gravitational waves. The tensor perturbations produce anisotropies and polarization which could generate measurable tensor power spectra. Here we explore how general gravitational waves affect CMB power spectra and present the constraints on the cosmological parameters in general states from the Planck satellite [24], the BICEP2 and Keck array through 2015 season (BK15) [25] and the Baryon Acoustic Oscillation (BAO) [26–28]. To achieve better constraints on the tensor power spectra parameters, observations should be combined at different frequency bands. The gravitational waves observations are considered which including the Laser Interferometer Gravitational-wave Observatory (LIGO) detector [29–31], the Laser Interferometer Space Antenna (LISA) detector [31, 32] and three Pulsar Timing Array (PTA) projects [33], namely the International Pulsar Timing Array (IPTA) [34], the Five-hundred-meter Aperture Spherical radio Telescope (FAST) [35] and the Square Kilometre Array (SKA) [36].

This paper is organized as follows. In section 2, we investigate the gravitational waves in general cosmological background. The equations and behaviors of gravitational waves are presented in general states. In section 3, the power spectra from tensor perturbations, namely TT spectrum, TE spectrum, EE spectrum and BB spectrum are explored in general states. In section 4, we represent the constraints on the cosmological parameters in general states from Planck+BK15+BAO datasets and measure the tensor power spectra parameters in general states from gravitational waves observations. A short summary and discussion are given in the last section.

---

\*Electronic address: [lijun@qust.edu.cn](mailto:lijun@qust.edu.cn)

## II. THE GRAVITATIONAL WAVES IN GENERAL COSMOLOGICAL BACKGROUND

The second-order perturbation metric about the Friedmann-Robert-Walker background in the conformal Newtonian gauge is taken as [37–39]

$$ds^2 = a^2 \left\{ -(1 + 2\phi)d\eta^2 + \left[ (1 - 2\phi)\delta_{ij} + \frac{h_{ij}}{2} \right] dx^i dx^j \right\}, \quad (1)$$

where  $a(\eta)$  is the scale factor,  $\eta$  is the conformal time,  $\phi$  is the scalar perturbation and  $h_{ij}$  is the gravitational waves perturbation. The energy momentum tensor of perfect fluid is given as

$$T_{\mu\nu} = (\rho + p)u_\mu u_\nu + pg_{\mu\nu}, \quad (2)$$

where  $\rho$  is the energy density and  $p$  is the pressure. The equation of state of the universe is given by

$$\omega = \rho/p, \quad (3)$$

where parameter  $\omega$  quantify the energy density compared to the pressure. In this paper, we focus on general state  $0 \leq \omega \leq 1$  as [10]. The matter domination, the radiation domination and the kinetic domination are corresponding to  $\omega = 0, 1/3, 1$  state respectively. When the universe is kinetic energy dominated, the scale factor grows as  $\eta^{\frac{1}{2}}$  as discussed in [40–42].

The gravitational waves satisfy following wave equations

$$h''_{ij} + \frac{4}{(1 + 3\omega)\eta} h'_{ij} - \Delta h_{ij} = 0, \quad (4)$$

where the prime denotes derivative with respect to conformal time and  $\Delta = \delta^{ij}\partial_i\partial_j$ . The contributions on the right hand side due to the anisotropic stress generated by neutrinos and photons are ignored. In the Fourier space, the equations become

$$h''_\lambda + \frac{4}{(1 + 3\omega)\eta} h'_\lambda + k^2 h_\lambda = 0. \quad (5)$$

The second damping terms are influenced by the state of universe  $\omega$ . The third dispersive terms affect the behaviors of gravitational waves by wavenumber  $k$ . The behaviors of gravitational waves  $h_\lambda(\eta)$  are illustrated in Fig. 1 which shows the larger value of  $\omega$ , the larger amplitude and frequency. The influence of general states are obvious in the propagation of gravitational waves. The modified gravitational waves propagation has been discussed as a powerful probe of modified gravity.

## III. THE POWER SPECTRA OF TENSOR PERTURBATIONS

The temperature and polarization perturbations generated by gravitational waves satisfy the following Boltz-

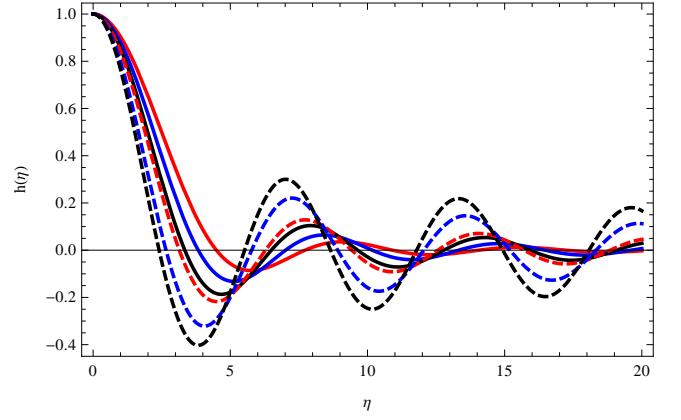


FIG. 1: The plot of gravitational waves  $h_\lambda(\eta)$  for  $\omega = \{0, 1/9, 1/4, 1/3, 2/3, 1\}$  in red, blue, black, dashed red, dashed blue and dashed black respectively.

mann equations

$$\tilde{\Delta}'_T{}^{(T)} + ik\mu\tilde{\Delta}_T{}^{(T)} = -h'_\lambda - \tau'[\tilde{\Delta}_T{}^{(T)} - \Psi], \quad (6)$$

$$\tilde{\Delta}'_P{}^{(T)} + ik\mu\tilde{\Delta}_P{}^{(T)} = -\tau'[\tilde{\Delta}_P{}^{(T)} + \Psi], \quad (7)$$

where

$$\Psi = \frac{\tilde{\Delta}_{T0}{}^{(T)}}{10} + \frac{\tilde{\Delta}_{T2}{}^{(T)}}{7} + \frac{3\tilde{\Delta}_{T4}{}^{(T)}}{70} - \frac{3\tilde{\Delta}_{P0}{}^{(T)}}{5} + \frac{6\tilde{\Delta}_{P2}{}^{(T)}}{7} - \frac{3\tilde{\Delta}_{P4}{}^{(T)}}{70},$$

the superscript  $(T)$  denotes contributions from tensor perturbations,  $\mu = \hat{n} \cdot \hat{k}$  is the angle between photon direction and wave vector,  $\tau'$  is the differential optical depth for Thomson scattering. The polarization perturbations which can be decomposed into E-mode and B-mode are produced by scalar perturbations and tensor perturbations. The B-mode components only come from tensor perturbations on the small multipoles and contains information of gravitational waves.

The anisotropy spectra and the polarization spectra are obtained by integrating over the initial power spectrum of metric perturbations

$$C_\ell^{(T)} = (4\pi)^2 \int k^2 dk P_h(k) \left| \Delta_{(T,P)\ell}^{(T)}(k, \eta = \eta_0) \right|^2. \quad (8)$$

The two-point correlations of temperature anisotropies and polarization patterns at different points in the sky are presented by Eq. (8). The tensor perturbations could generate measurable CMB power spectra.

In order to obtain numerical results for CMB angular power spectra from general gravitational waves, we modify CAMB [43] by taking into account the evolution equations for tensor perturbations in Eq. (5). We represent the tensor power spectra in general states in Fig. 2 which shows any modification of gravitational waves can potentially lead to observable effect on CMB temperature and polarization spectra. These signatures match the analytic results of gravitational waves in Fig. 1.

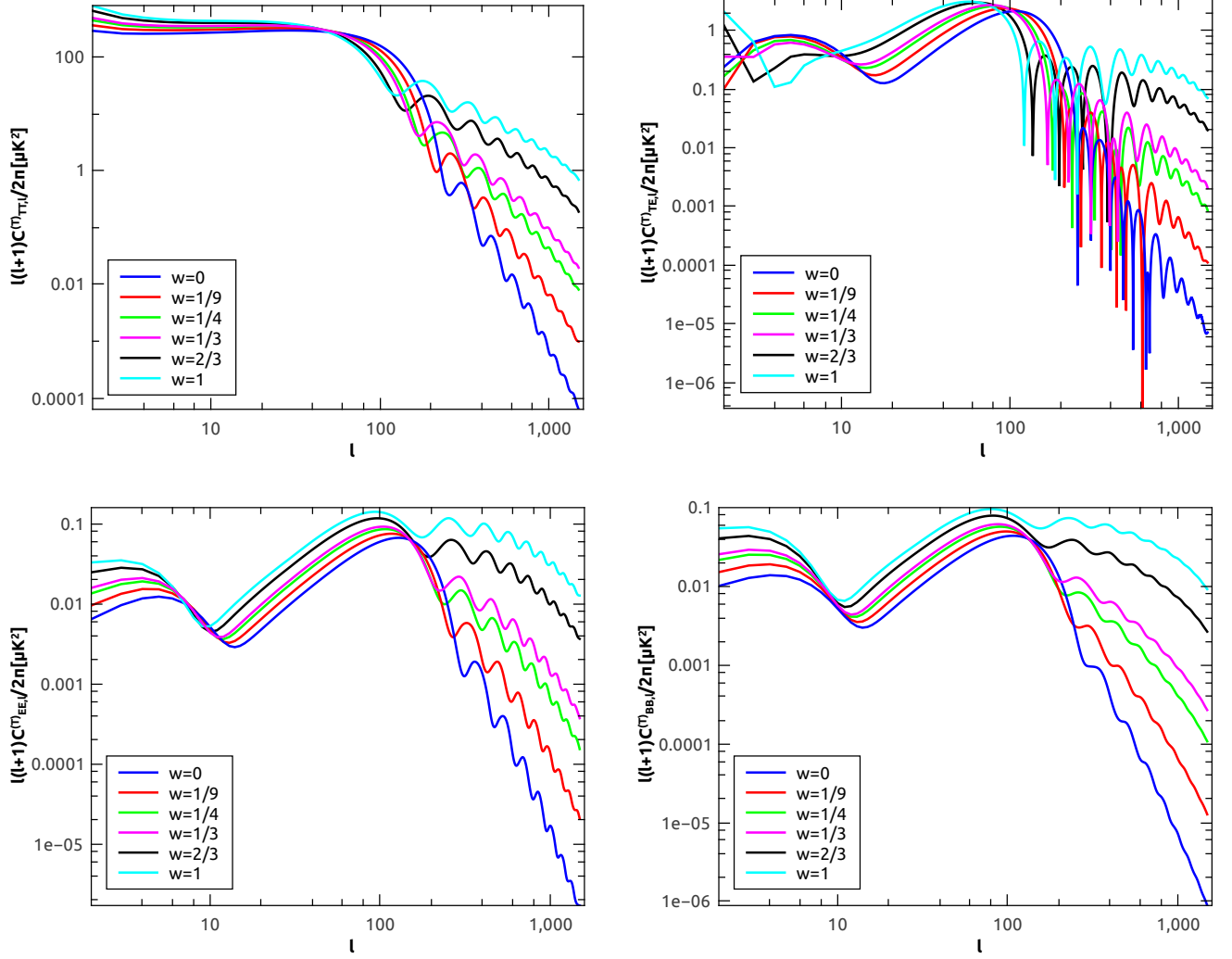


FIG. 2: The plots of TT, TE, EE and BB power spectra from tensor perturbations for  $\omega = \{0, 1/9, 1/4, 1/3, 2/3, 1\}$  respectively.

In the TT power spectra, the curve becomes higher with larger value of  $\omega$  for low CMB multipoles  $\ell \lesssim 40$ . When the multipole is nearly  $\ell \simeq 50$ , all the curves fix on one point. Curves begin oscillating for  $100 \lesssim \ell \lesssim 1000$  multipoles and  $\omega = 1$  state is the first one to oscillate. The TT power spectrum of  $\omega = 1$  state is nearly  $10^4$  times larger than that of  $\omega = 0$  state for  $\ell \simeq 1000$ . The TT power spectra are much larger than any other three tensor power spectra.

In the TE power spectra, the first peaks are coming from low CMB multipoles  $0 \lesssim \ell \lesssim 15$  except  $\omega = 2/3$  state and  $\omega = 1$  state. The second peaks are in  $15 \lesssim \ell \lesssim 120$  multipoles and  $\omega = 1$  state is the highest one. Curves begin oscillating for  $120 \lesssim \ell \lesssim 1000$  multipoles and  $\omega = 1$  state is the first one to oscillate. The TE power spectrum of  $\omega = 1$  state is nearly  $10^4$  times larger than that of  $\omega = 0$  state for  $\ell \simeq 1000$ . The curves in the oscillatory multipoles alter severest in the TE power spectra comparing with any other three tensor power spectra.

In the EE power spectra, the larger value of  $\omega$ , the earlier coming and larger value of the first peak for low CMB multipoles  $0 \lesssim \ell \lesssim 10$ . The second peaks are in  $10 \lesssim \ell \lesssim 120$  multipoles and the second peak of  $\omega = 1$  state is the highest. Curves begin to oscillate for  $120 \lesssim \ell \lesssim 1000$  multipoles. The EE power spectrum of  $\omega = 1$  state is nearly  $10^3$  times larger than that of  $\omega = 0$  state for  $\ell \simeq 1000$ . The EE power spectra are much smaller than the TT power spectra.

In the BB power spectra, the behaviors are similar with the EE power spectra. The larger value of  $\omega$ , the earlier coming and larger value of the first peak for low CMB multipoles  $0 \lesssim \ell \lesssim 10$ . The second peaks are in  $10 \lesssim \ell \lesssim 120$  multipoles and  $\omega = 1$  state is the highest one. Curves begin to oscillate for  $120 \lesssim \ell \lesssim 1000$  multipoles. The BB power spectrum of  $\omega = 1$  state is nearly  $10^4$  times larger than that of  $\omega = 0$  state for  $\ell \simeq 1000$  which is much smaller than the TT power spectra.

#### IV. THE CONSTRAINTS ON THE COSMOLOGICAL PARAMETERS IN GENERAL STATES

The power spectra of scalar and tensor perturbations are parameterized by

$$P_s(k) = A_s \left( \frac{k}{k_*} \right)^{n_s-1}, \quad (9)$$

$$P_t(k) = A_t \left( \frac{k}{k_*} \right)^{n_t}, \quad (10)$$

where  $A_s$  and  $A_t$  are the scalar and tensor amplitude at the pivot scale  $k_* = 0.05 \text{ Mpc}^{-1}$ ,  $n_s$  is the scalar spectral index and  $n_t$  is the tensor spectral index. Usually we introduce a new parameter, namely the tensor-to-scalar ratio  $r$ , to quantify the tensor amplitude compared to the scalar amplitude at the pivot scale:

$$r \equiv \frac{A_t}{A_s}. \quad (11)$$

It is known that the single parameter Harrison-Zeldovich spectrum ( $n_s = 1$ ) does not fit the data and at least the parameters  $A_s$  and  $n_s$  in the expansion of the scalar power spectrum are needed.

In the standard  $\Lambda\text{CDM}$  model, the six parameters are the baryon density parameter  $\Omega_b h^2$ , the cold dark matter density  $\Omega_c h^2$ , the angular size of the horizon at the last scattering surface  $\theta_{\text{MC}}$ , the optical depth  $\tau$ , the scalar amplitude  $A_s$  and the scalar spectral index  $n_s$ . First, we extend this scenario by adding the tensor-to-scalar ratio  $r$  and constrain these seven cosmological parameters in the  $\Lambda\text{CDM}+r$  model from Planck+BK15+BAO datasets. The spectral index of tensor power spectra is set as  $n_t = -r/8$  which is nothing but the consistency relation to lowest order in the single-field slow-roll inflation model [44, 45]. Here we use the publicly available codes Cosmomc [46] to constrain these seven cosmological parameters within the evolution equations of general gravitational waves from tensor perturbations in Eq. (5). The numerical results are presented in Table. I, Fig. 3 and Fig. 4.

In the  $\Lambda\text{CDM}+r$  model, the constraints on the scalar spectral index  $n_s$  and the tensor-to-scalar ratio  $r$  are

$$n_s = 0.9654 \pm 0.0037 \quad (68\% \text{ C.L.}), \quad (12)$$

$$r < 0.075 \quad (95\% \text{ C.L.}), \quad (13)$$

from Planck+BK15+BAO datasets for  $\omega = 0$  state. The constraints on the scalar spectral index  $n_s$  and the tensor-to-scalar ratio  $r$  become

$$n_s = 0.9654 \pm 0.0038 \quad (68\% \text{ C.L.}), \quad (14)$$

$$r < 0.074 \quad (95\% \text{ C.L.}), \quad (15)$$

from Planck+BK15+BAO datasets for  $\omega = 1/9$  state. The constraints on the scalar spectral index  $n_s$  and the

tensor-to-scalar ratio  $r$  are

$$n_s = 0.9654 \pm 0.0038 \quad (68\% \text{ C.L.}), \quad (16)$$

$$r < 0.073 \quad (95\% \text{ C.L.}), \quad (17)$$

from Planck+BK15+BAO datasets for  $\omega = 1/4$  state. The constraints on the scalar spectral index  $n_s$  and the tensor-to-scalar ratio  $r$  become

$$n_s = 0.9655 \pm 0.0037 \quad (68\% \text{ C.L.}), \quad (18)$$

$$r < 0.071 \quad (95\% \text{ C.L.}), \quad (19)$$

from Planck+BK15+BAO datasets for  $\omega = 1/3$  state. The constraints on the scalar spectral index  $n_s$  and the tensor-to-scalar ratio  $r$  are

$$n_s = 0.9655^{+0.0038}_{-0.0037} \quad (68\% \text{ C.L.}), \quad (20)$$

$$r < 0.074 \quad (95\% \text{ C.L.}), \quad (21)$$

from Planck+BK15+BAO datasets for  $\omega = 2/3$  state. The constraints on the scalar spectral index  $n_s$  and the tensor-to-scalar ratio  $r$  become

$$n_s = 0.9656 \pm 0.0038 \quad (68\% \text{ C.L.}), \quad (22)$$

$$r < 0.075 \quad (95\% \text{ C.L.}), \quad (23)$$

from Planck+BK15+BAO datasets for  $\omega = 1$  state. The numerical results show that the general states have significant impacts on the tensor-to-scalar ratio. The marginalized contour plot for parameters  $n_s$  and  $r$  in the  $\Lambda\text{CDM}+r$  model at the 68% and 95% CL are given in Fig. 4 from the combinations of Planck+BK15+BAO for general states respectively which can be used to select inflation models as [47–56].

Here we compare some inflation models depending on the marginalized contour plot for parameters  $n_s$  and  $r$  from Planck+BK15+BAO datasets. In the  $V(\phi) \propto \phi^n$  inflation model [49], the scalar spectral index and tensor-to-scalar ratio at first order are

$$n_s \approx 1 - \frac{2(n+2)}{4N+n}, \quad (24)$$

$$r \approx \frac{16n}{4N+n}, \quad (25)$$

where  $N$  is the e-folding number. In the Starobinsky inflation model [50] which computes for the  $R^2$  theory, the scalar spectral index and tensor-to-scalar ratio take the form

$$n_s \approx 1 - \frac{2}{N}, \quad (26)$$

$$r \approx \frac{12}{N^2}. \quad (27)$$

In the spontaneously broken SUSY (SBS) inflation model [51–55], the scalar spectral index and tensor-to-scalar ratio are given by

$$r \approx 0, \quad (28)$$

$$n_s \approx 1 - \frac{1}{N}. \quad (29)$$



Parameters	Planck+BK15 +BAO( $\omega = 0$ )	Planck+BK15 +BAO( $\omega = 1/9$ )	Planck+BK15 +BAO( $\omega = 1/4$ )	Planck+BK15 +BAO( $\omega = 1/3$ )	Planck+BK15 +BAO( $\omega = 2/3$ )	Planck+BK15 +BAO( $\omega = 1$ )
$\Omega_b h^2$	$0.02240 \pm 0.00013$	$0.02241 \pm 0.00013$	$0.02240 \pm 0.00013$	$0.02240 \pm 0.00013$	$0.02241 \pm 0.00013$	$0.02240 \pm 0.00014$
$\Omega_c h^2$	$0.11956 \pm 0.00091$	$0.11958^{+0.00093}_{-0.00092}$	$0.11959^{+0.00092}_{-0.00093}$	$0.11957^{+0.00090}_{-0.00093}$	$0.11958^{+0.00093}_{-0.00092}$	$0.11956^{+0.00093}_{-0.00094}$
$100\theta_{MC}$	$1.04099 \pm 0.00028$	$1.04099 \pm 0.00029$	$1.04099 \pm 0.00029$	$1.04099 \pm 0.00029$	$1.04100 \pm 0.00028$	$1.04098 \pm 0.00030$
$\tau$	$0.0568^{+0.0070}_{-0.0076}$	$0.0569^{+0.0068}_{-0.0079}$	$0.0568^{+0.0070}_{-0.0077}$	$0.0569^{+0.0068}_{-0.0074}$	$0.0566^{+0.0069}_{-0.0077}$	$0.0568 \pm 0.0071$
$\ln(10^{10} A_s)$	$3.049 \pm 0.014$	$3.049^{+0.014}_{-0.015}$	$3.049 \pm 0.014$	$3.049 \pm 0.014$	$3.049 \pm 0.014$	$3.049^{+0.014}_{-0.015}$
$n_s$	$0.9654 \pm 0.0037$	$0.9654 \pm 0.0038$	$0.9654 \pm 0.0038$	$0.9655 \pm 0.0037$	$0.9655^{+0.0038}_{-0.0037}$	$0.9656 \pm 0.0038$
$r_{0.05}$	$< 0.075$	$< 0.074$	$< 0.073$	$< 0.071$	$< 0.074$	$< 0.075$

TABLE I: The 68% limits on the standard cosmological parameters and the 95% limits on the tensor-to-scalar ratio in the  $\Lambda$ CDM+ $r$  model from the combinations of Planck+BK15+BAO for  $\omega = \{0, 1/9, 1/4, 1/3, 2/3, 1\}$  respectively.

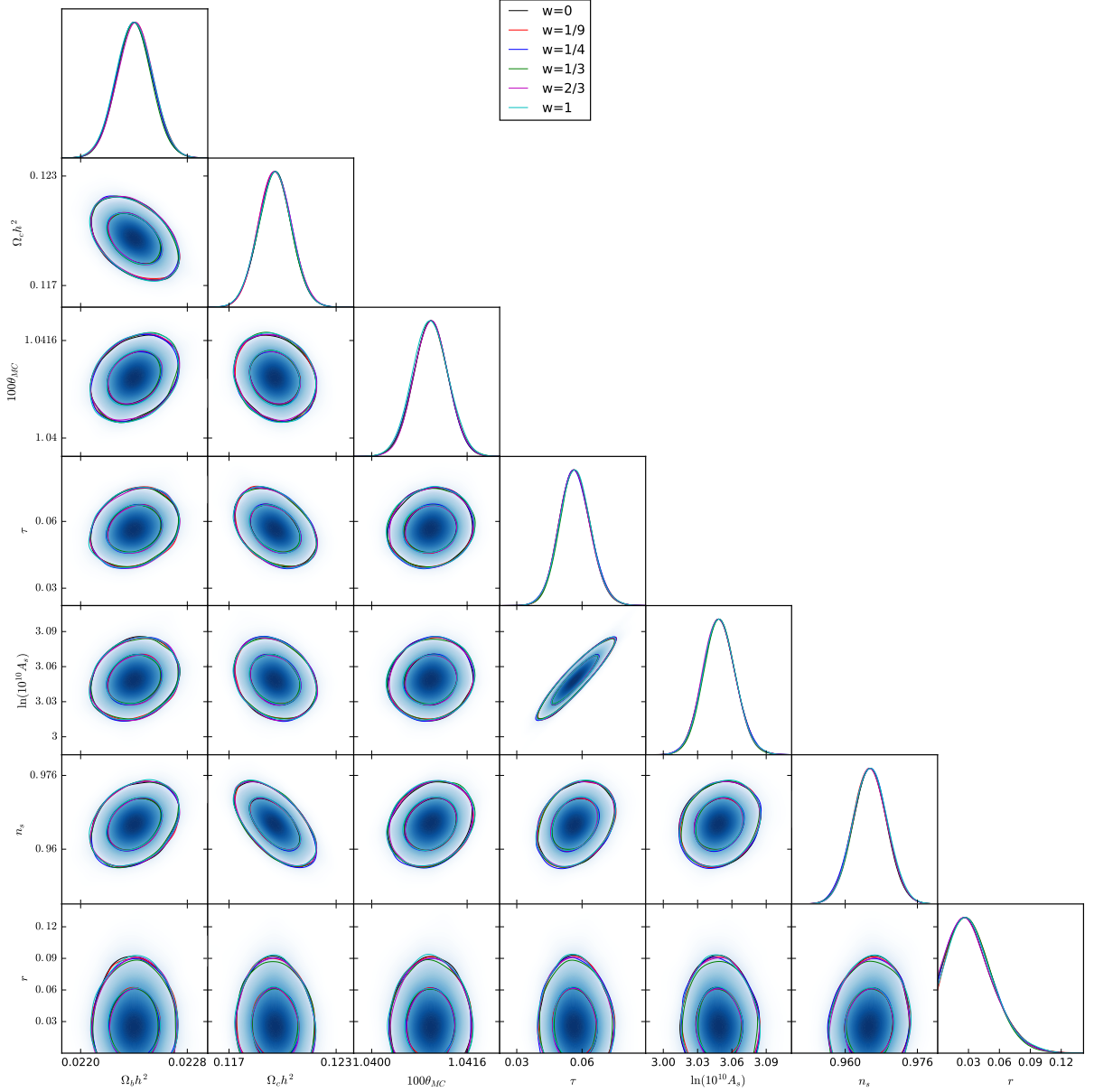


FIG. 3: The contour plots and the likelihood distributions for the seven cosmological parameters in the  $\Lambda$ CDM+ $r$  model at the 68% and 95% CL from the combinations of Planck+BK15+BAO for  $\omega = \{0, 1/9, 1/4, 1/3, 2/3, 1\}$  respectively.

In the superconformal inflationary  $\alpha$ -attractors [56] which introduces parameter  $\alpha$  inversely proportional to

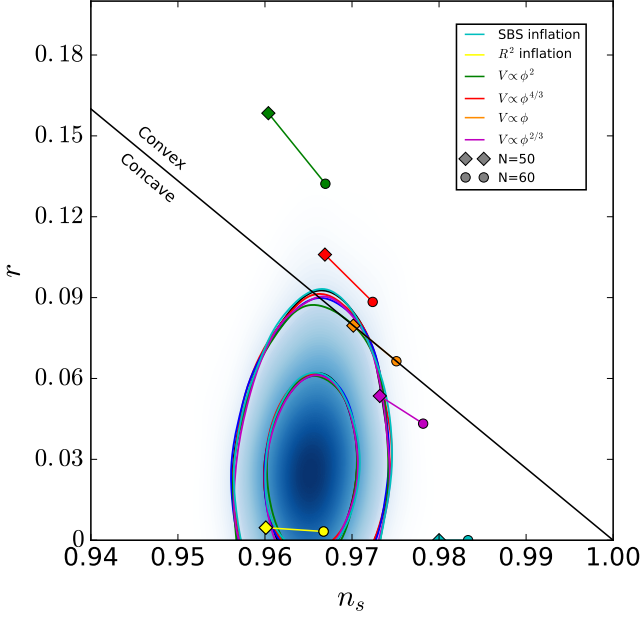


FIG. 4: The marginalized contour plot for parameters  $n_s$  and  $r$  in the  $\Lambda$ CDM+ $r$  model at the 68% and 95% CL from the combinations of Planck+BK15+BAO for  $\omega = \{0, 1/9, 1/4, 1/3, 2/3, 1\}$  in black, red, dark blue, green, purple and light blue respectively.

the curvature of the inflaton Kähler manifold, the scalar spectral index and tensor-to-scalar ratio are given by

$$n_s = 1 - \frac{2}{N}, \quad (30)$$

$$r = \alpha \frac{12}{N^2}. \quad (31)$$

When we choose appropriate value for  $\alpha$ , it could become the Starobinsky inflation model or the  $V(\phi) \propto \phi^2$  inflation model. Depend on these relations of parameters  $n_s$  and  $r$ , we find that the Starobinsky inflation model fit the Planck+BK15+BAO datasets better.

Then we measure the tensor power spectra parameters in general states from gravitational waves observations which including LIGO, LISA, IPTA, FAST and SKA projects and taking the same method by the signal-to-noise ratio and stochastic gravitational wave background as our previous works [57–59]. We fix the standard  $\Lambda$ CDM parameters based on Table. I and consider the tensor-to-scalar ratio  $r$  and the tensor spectral index  $n_t$  as fully free parameters. The numerical results are presented in Table. II, Fig. 5 and Fig. 6.

In the  $\Lambda$ CDM+ $r+n_t$  model, the constraints on parameters  $r$  and  $n_t$  are given by

$$r < 0.121 \quad (95\% \text{ C.L.}), \quad (32)$$

$$n_t = 0.0605^{+0.47}_{-0.14} \quad (95\% \text{ C.L.}), \quad (33)$$

from BK15+LIGO datasets for  $\omega = 0$  state. The con-

straints on parameters  $r$  and  $n_t$  are given by

$$r < 0.115 \quad (95\% \text{ C.L.}), \quad (34)$$

$$n_t = 0.0467^{+0.48}_{-0.13} \quad (95\% \text{ C.L.}), \quad (35)$$

from BK15+LIGO datasets for  $\omega = 1/9$  state. The constraints on parameters  $r$  and  $n_t$  are given by

$$r < 0.117 \quad (95\% \text{ C.L.}), \quad (36)$$

$$n_t = 0.0230^{+0.51}_{-0.15} \quad (95\% \text{ C.L.}), \quad (37)$$

from BK15+LIGO datasets for  $\omega = 1/4$  state. The constraints on parameters  $r$  and  $n_t$  are given by

$$r < 0.121 \quad (95\% \text{ C.L.}), \quad (38)$$

$$n_t = 0.0079^{+0.53}_{-0.12} \quad (95\% \text{ C.L.}), \quad (39)$$

from BK15+LIGO datasets for  $\omega = 1/3$  state. The constraints on parameters  $r$  and  $n_t$  are given by

$$r < 0.114 \quad (95\% \text{ C.L.}), \quad (40)$$

$$n_t = 0.0479^{+0.50}_{-0.15} \quad (95\% \text{ C.L.}), \quad (41)$$

from BK15+LIGO datasets for  $\omega = 2/3$  state. The constraints on parameters  $r$  and  $n_t$  are given by

$$r < 0.120 \quad (95\% \text{ C.L.}), \quad (42)$$

$$n_t = 0.0091^{+0.53}_{-0.12} \quad (95\% \text{ C.L.}), \quad (43)$$

from BK15+LIGO datasets for  $\omega = 1$  state.

We also predict the detect ability of LISA. We assume that the stochastic gravitational wave background cannot be detected using LISA or PTA, and observe how these data will potentially improve constraints on the tensor tilt. The constraints on parameters  $r$  and  $n_t$  are given by

$$r < 0.080 \quad (95\% \text{ C.L.}), \quad (44)$$

$$n_t = -0.1857^{+0.47}_{-0.14} \quad (95\% \text{ C.L.}), \quad (45)$$

from BK15+LISA datasets for  $\omega = 0$  state. The constraints on parameters  $r$  and  $n_t$  are given by

$$r < 0.076 \quad (95\% \text{ C.L.}), \quad (46)$$

$$n_t = -0.2058^{+0.50}_{-0.14} \quad (95\% \text{ C.L.}), \quad (47)$$

from BK15+LISA datasets for  $\omega = 1/9$  state. The constraints on parameters  $r$  and  $n_t$  are given by

$$r < 0.077 \quad (95\% \text{ C.L.}), \quad (48)$$

$$n_t = -0.2017^{+0.49}_{-0.13} \quad (95\% \text{ C.L.}), \quad (49)$$

from BK15+LISA datasets for  $\omega = 1/4$  state. The constraints on parameters  $r$  and  $n_t$  are given by

$$r < 0.081 \quad (95\% \text{ C.L.}), \quad (50)$$

$$n_t = -0.1951^{+0.48}_{-0.15} \quad (95\% \text{ C.L.}), \quad (51)$$

States	Parameters	BK15+LIGO	BK15+LISA	BK15+IPTA	BK15+FAST	BK15+SKA
$\omega = 0$	$r_{0.05}$	$< 0.121$	$< 0.080$	$< 0.084$	$< 0.057$	$< 0.030$
	$n_t$	$0.0605^{+0.47}_{-0.14}$	$-0.1857^{+0.47}_{-0.14}$	$-0.1473^{+0.53}_{-0.15}$	$-0.3982^{+0.48}_{-0.15}$	$-0.7432^{+0.54}_{-0.15}$
$\omega = 1/9$	$r_{0.05}$	$< 0.115$	$< 0.076$	$< 0.086$	$< 0.050$	$< 0.030$
	$n_t$	$0.0467^{+0.48}_{-0.13}$	$-0.2058^{+0.50}_{-0.14}$	$-0.1273^{+0.51}_{-0.15}$	$-0.3913^{+0.47}_{-0.16}$	$-0.7300^{+0.53}_{-0.16}$
$\omega = 1/4$	$r_{0.05}$	$< 0.117$	$< 0.077$	$< 0.084$	$< 0.052$	$< 0.029$
	$n_t$	$0.0230^{+0.51}_{-0.15}$	$-0.2017^{+0.49}_{-0.13}$	$-0.1178^{+0.50}_{-0.15}$	$-0.4295^{+0.52}_{-0.14}$	$-0.7489^{+0.54}_{-0.16}$
$\omega = 1/3$	$r_{0.05}$	$< 0.121$	$< 0.081$	$< 0.084$	$< 0.052$	$< 0.029$
	$n_t$	$0.0079^{+0.53}_{-0.12}$	$-0.1951^{+0.48}_{-0.15}$	$-0.1280^{+0.51}_{-0.15}$	$-0.4431^{+0.54}_{-0.15}$	$-0.7468^{+0.54}_{-0.15}$
$\omega = 2/3$	$r_{0.05}$	$< 0.114$	$< 0.074$	$< 0.083$	$< 0.052$	$< 0.028$
	$n_t$	$0.0479^{+0.50}_{-0.15}$	$-0.2623^{+0.57}_{-0.14}$	$-0.1238^{+0.50}_{-0.15}$	$-0.3935^{+0.47}_{-0.15}$	$-0.7229^{+0.51}_{-0.16}$
$\omega = 1$	$r_{0.05}$	$< 0.120$	$< 0.077$	$< 0.087$	$< 0.053$	$< 0.030$
	$n_t$	$0.0091^{+0.53}_{-0.12}$	$-0.1990^{+0.49}_{-0.14}$	$-0.1331^{+0.51}_{-0.16}$	$-0.4191^{+0.51}_{-0.15}$	$-0.7358^{+0.51}_{-0.17}$

TABLE II: The 95% limits on the tensor-to-scalar ratio  $r$  and the tensor spectral index  $n_t$  in the  $\Lambda$ CDM+ $r+n_t$  model for general states from the combinations of BK15+LIGO, BK15+LISA, BK15+IPTA, BK15+FAST and BK15+SKA respectively.

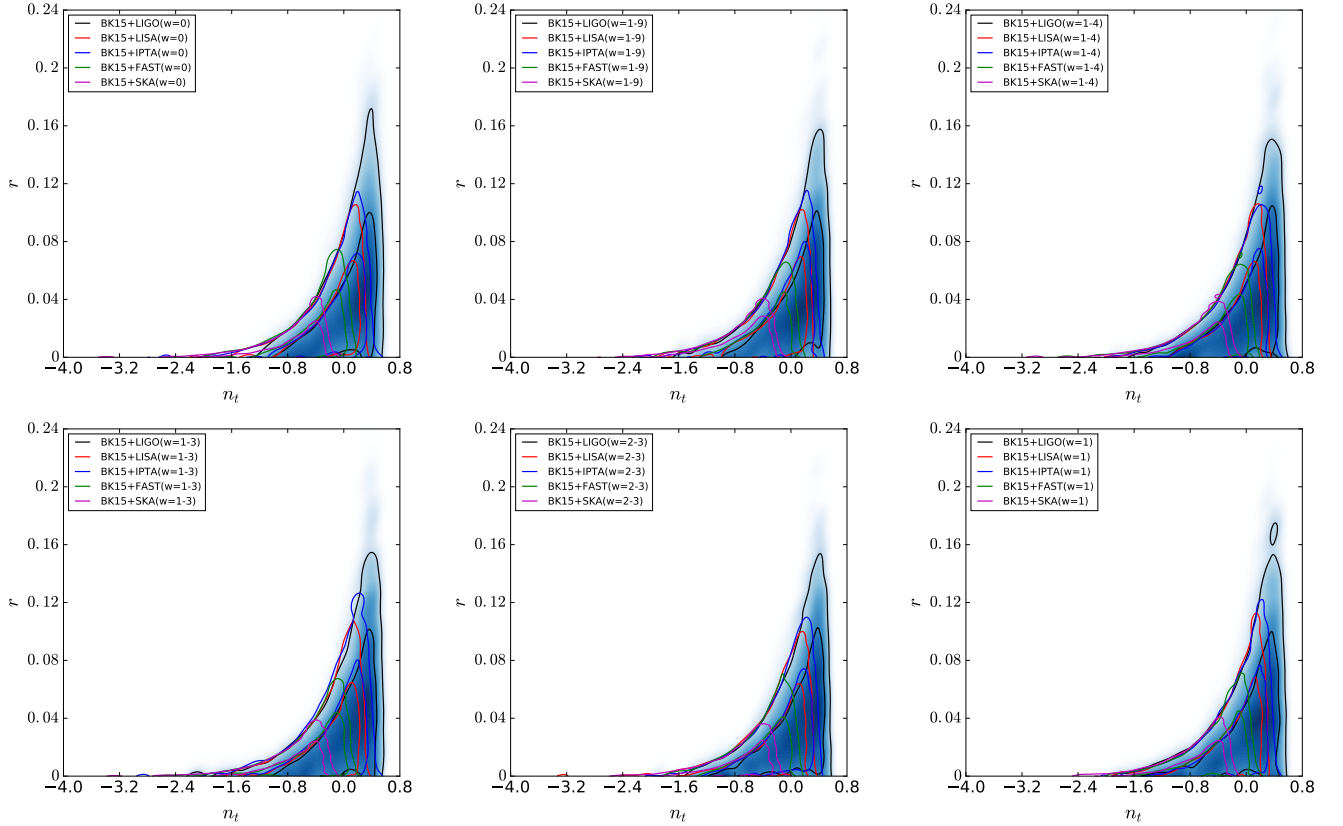


FIG. 5: The marginalized contour plot for parameters  $n_t$  and  $r$  in the  $\Lambda$ CDM+ $r+n_t$  model at the 68% and 95% CL from the combinations of BK15+LIGO, BK15+LISA, BK15+IPTA, BK15+FAST and BK15+SKA according to the state of the universe  $\omega = \{0, 1/9, 1/4, 1/3, 2/3, 1\}$  respectively.

from BK15+LISA datasets for  $\omega = 1/3$  state. The constraints on parameters  $r$  and  $n_t$  are given by

$$r < 0.074 \quad (95\% \text{ C.L.}), \quad (52)$$

$$n_t = -0.2623^{+0.57}_{-0.14} \quad (95\% \text{ C.L.}), \quad (53)$$

from BK15+LISA datasets for  $\omega = 2/3$  state. The con-

straints on parameters  $r$  and  $n_t$  are given by

$$r < 0.077 \quad (95\% \text{ C.L.}), \quad (54)$$

$$n_t = -0.1990^{+0.49}_{-0.14} \quad (95\% \text{ C.L.}), \quad (55)$$

from BK15+LISA datasets for  $\omega = 1$  state.

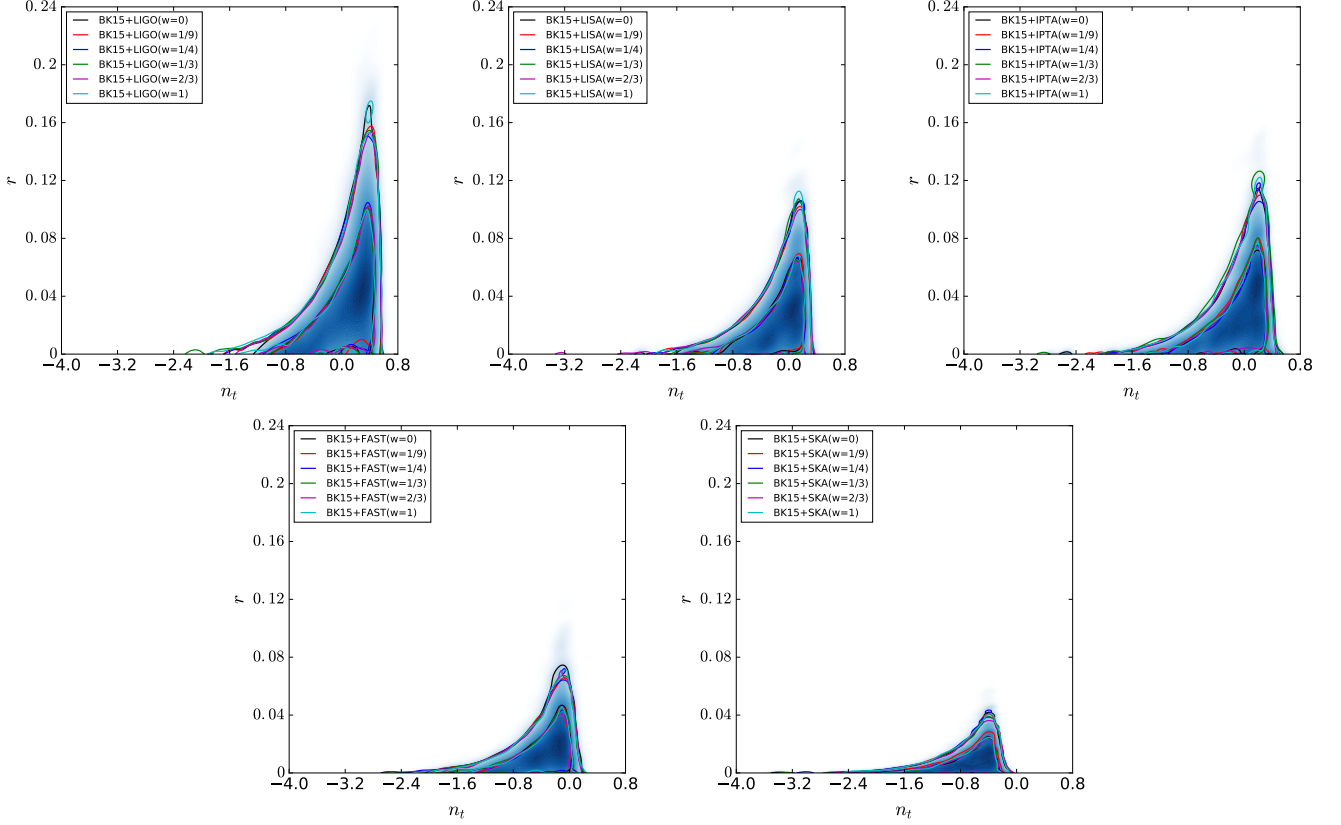


FIG. 6: The marginalized contour plot for parameters  $n_t$  and  $r$  in the  $\Lambda\text{CDM}+r+n_t$  model at the 68% and 95% CL from the combinations of BK15+LIGO, BK15+LISA, BK15+IPTA, BK15+FAST and BK15+SKA for  $\omega = \{0, 1/9, 1/4, 1/3, 2/3, 1\}$  respectively.

We also predict the detect ability of PTA. The constraints on parameters  $r$  and  $n_t$  are given by

$$r < 0.084 \quad (95\% \text{ C.L.}), \quad (56)$$

$$n_t = -0.1473^{+0.53}_{-0.15} \quad (95\% \text{ C.L.}), \quad (57)$$

from BK15+IPTA datasets for  $\omega = 0$  state. The constraints on parameters  $r$  and  $n_t$  are given by

$$r < 0.086 \quad (95\% \text{ C.L.}), \quad (58)$$

$$n_t = -0.1273^{+0.51}_{-0.15} \quad (95\% \text{ C.L.}), \quad (59)$$

from BK15+IPTA datasets for  $\omega = 1/9$  state. The constraints on parameters  $r$  and  $n_t$  are given by

$$r < 0.084 \quad (95\% \text{ C.L.}), \quad (60)$$

$$n_t = -0.1178^{+0.50}_{-0.15} \quad (95\% \text{ C.L.}), \quad (61)$$

from BK15+IPTA datasets for  $\omega = 1/4$  state. The constraints on parameters  $r$  and  $n_t$  are given by

$$r < 0.084 \quad (95\% \text{ C.L.}), \quad (62)$$

$$n_t = -0.1280^{+0.51}_{-0.15} \quad (95\% \text{ C.L.}), \quad (63)$$

from BK15+IPTA datasets for  $\omega = 1/3$  state. The constraints on parameters  $r$  and  $n_t$  are given by

$$r < 0.083 \quad (95\% \text{ C.L.}), \quad (64)$$

$$n_t = -0.1238^{+0.50}_{-0.15} \quad (95\% \text{ C.L.}), \quad (65)$$

from BK15+IPTA datasets for  $\omega = 2/3$  state. The constraints on parameters  $r$  and  $n_t$  are given by

$$r < 0.087 \quad (95\% \text{ C.L.}), \quad (66)$$

$$n_t = -0.1331^{+0.51}_{-0.16} \quad (95\% \text{ C.L.}), \quad (67)$$

from BK15+IPTA datasets for  $\omega = 1$  state.

The constraints on parameters  $r$  and  $n_t$  are given by

$$r < 0.057 \quad (95\% \text{ C.L.}), \quad (68)$$

$$n_t = -0.3982^{+0.48}_{-0.15} \quad (95\% \text{ C.L.}), \quad (69)$$

from BK15+FAST datasets for  $\omega = 0$  state. The constraints on parameters  $r$  and  $n_t$  are given by

$$r < 0.050 \quad (95\% \text{ C.L.}), \quad (70)$$

$$n_t = -0.3913^{+0.47}_{-0.16} \quad (95\% \text{ C.L.}), \quad (71)$$

from BK15+FAST datasets for  $\omega = 1/9$  state. The constraints on parameters  $r$  and  $n_t$  are given by

$$r < 0.052 \quad (95\% \text{ C.L.}), \quad (72)$$

$$n_t = -0.4295^{+0.52}_{-0.14} \quad (95\% \text{ C.L.}), \quad (73)$$

from BK15+FAST datasets for  $\omega = 1/4$  state. The constraints on parameters  $r$  and  $n_t$  are given by

$$r < 0.052 \quad (95\% \text{ C.L.}), \quad (74)$$

$$n_t = -0.4431^{+0.54}_{-0.15} \quad (95\% \text{ C.L.}), \quad (75)$$

from BK15+FAST datasets for  $\omega = 1/3$  state. The constraints on parameters  $r$  and  $n_t$  are given by

$$r < 0.052 \quad (95\% \text{ C.L.}), \quad (76)$$

$$n_t = -0.3935^{+0.47}_{-0.15} \quad (95\% \text{ C.L.}), \quad (77)$$

from BK15+FAST datasets for  $\omega = 2/3$  state. The constraints on parameters  $r$  and  $n_t$  are given by

$$r < 0.053 \quad (95\% \text{ C.L.}), \quad (78)$$

$$n_t = -0.4191^{+0.51}_{-0.15} \quad (95\% \text{ C.L.}), \quad (79)$$

from BK15+FAST datasets for  $\omega = 1$  state.

The constraints on parameters  $r$  and  $n_t$  are given by

$$r < 0.030 \quad (95\% \text{ C.L.}), \quad (80)$$

$$n_t = -0.7432^{+0.54}_{-0.15} \quad (95\% \text{ C.L.}), \quad (81)$$

from BK15+SKA datasets for  $\omega = 0$  state. The constraints on parameters  $r$  and  $n_t$  are given by

$$r < 0.030 \quad (95\% \text{ C.L.}), \quad (82)$$

$$n_t = -0.7300^{+0.53}_{-0.16} \quad (95\% \text{ C.L.}), \quad (83)$$

from BK15+SKA datasets for  $\omega = 1/9$  state. The constraints on parameters  $r$  and  $n_t$  are given by

$$r < 0.029 \quad (95\% \text{ C.L.}), \quad (84)$$

$$n_t = -0.7489^{+0.54}_{-0.16} \quad (95\% \text{ C.L.}), \quad (85)$$

from BK15+SKA datasets for  $\omega = 1/4$  state. The constraints on parameters  $r$  and  $n_t$  are given by

$$r < 0.029 \quad (95\% \text{ C.L.}), \quad (86)$$

$$n_t = -0.7468^{+0.54}_{-0.15} \quad (95\% \text{ C.L.}), \quad (87)$$

from BK15+SKA datasets for  $\omega = 1/3$  state. The constraints on parameters  $r$  and  $n_t$  are given by

$$r < 0.028 \quad (95\% \text{ C.L.}), \quad (88)$$

$$n_t = -0.7229^{+0.51}_{-0.16} \quad (95\% \text{ C.L.}), \quad (89)$$

from BK15+SKA datasets for  $\omega = 2/3$  state. The constraints on parameters  $r$  and  $n_t$  are given by

$$r < 0.030 \quad (95\% \text{ C.L.}), \quad (90)$$

$$n_t = -0.7358^{+0.51}_{-0.17} \quad (95\% \text{ C.L.}), \quad (91)$$

from BK15+SKA datasets for  $\omega = 1$  state. These results are illustrated in Table. II, Fig. 5 and Fig. 6.

## V. SUMMARY

In this paper, we consider how general gravitational waves affect CMB power spectra and explore the constraints on the cosmological parameters in general states from Planck+BK15+BAO datasets. In the  $\Lambda$ CDM+ $r$  model, the impacts on the tensor-to-scalar ratio are obvious. We also measure the tensor power spectra parameters in general states from gravitational waves observations within LIGO, LISA, IPTA, FAST and SKA projects and find that these data can significantly improve constraints on the tensor tilt if the amplitude of the tensor power spectrum is within the detectable range. In particular, compared with LIGO and LISA, SKA may provide a much better constraint on the positive part of the tensor tilt.

We look forward to use the available data from the BICEP/Keck Observations through the 2018 Observing Season (BK18) [60] to obtain better constraints on the tensor power spectra parameters.

- 
- [1] A. H. Guth, Phys. Rev. D **23** (1981), 347-356
  - [2] A. Riotto, ICTP Lect. Notes Ser. **14** (2003), 317-413 [arXiv:hep-ph/0210162 [hep-ph]].
  - [3] M. Kamionkowski, A. Kosowsky and A. Stebbins, Phys. Rev. Lett. **78** (1997), 2058-2061 [arXiv:astro-ph/9609132 [astro-ph]].
  - [4] P. Cabella and M. Kamionkowski, [arXiv:astro-ph/0403392 [astro-ph]].
  - [5] A. Kosowsky, New Astron. Rev. **43** (1999), 157 [arXiv:astro-ph/9904102 [astro-ph]].
  - [6] M. Kamionkowski and E. D. Kovetz, Ann. Rev. Astron. Astrophys. **54** (2016), 227-269 [arXiv:1510.06042 [astro-ph.CO]].
  - [7] S. Chandrasekhar, Radiation Transfer (Dover, 1960).
  - [8] C. T. Byrnes, M. Hindmarsh, S. Young and M. R. S. Hawkins, JCAP **08** (2018), 041 [arXiv:1801.06138 [astro-ph.CO]].
  - [9] F. Hajkarim and J. Schaffner-Bielich, Phys. Rev. D **101** (2020) no.4, 043522 [arXiv:1910.12357 [hep-ph]].
  - [10] G. Domènech, Int. J. Mod. Phys. D **29** (2020) no.03, 2050028 [arXiv:1912.05583 [gr-qc]].
  - [11] J. Li and Q. G. Huang, JCAP **02** (2018), 020 [arXiv:1712.07771 [astro-ph.CO]].
  - [12] Y. F. Cai, C. Lin, B. Wang and S. F. Yan, Phys. Rev. Lett. **126** (2021) no.7, 071303 [arXiv:2009.09833 [gr-qc]].
  - [13] Y. Di, J. Wang, R. Zhou, L. Bian, R. G. Cai and J. Liu, Phys. Rev. Lett. **126** (2021) no.25, 251102 [arXiv:2012.15625 [astro-ph.CO]].



- [14] Z. Z. Peng, C. Fu, J. Liu, Z. K. Guo and R. G. Cai, [arXiv:2106.11816 [astro-ph.CO]].
- [15] S. Dubovsky, R. Flauger, A. Starobinsky and I. Tkachev, Phys. Rev. D **81** (2010), 023523 [arXiv:0907.1658 [astro-ph.CO]].
- [16] W. Lin and M. Ishak, Phys. Rev. D **94** (2016) no.12, 123011 [arXiv:1605.03504 [astro-ph.CO]].
- [17] P. Brax, S. Cespedes and A. C. Davis, JCAP **03** (2018), 008 [arXiv:1710.09818 [astro-ph.CO]].
- [18] L. Amendola, G. Ballesteros and V. Pettorino, Phys. Rev. D **90** (2014), 043009 [arXiv:1405.7004 [astro-ph.CO]].
- [19] L. Boubekeur, E. Giusarma, O. Mena and H. Ramírez, Phys. Rev. D **90** (2014) no.10, 103512 [arXiv:1407.6837 [astro-ph.CO]].
- [20] M. Fasiello and R. H. Ribeiro, JCAP **07** (2015), 027 [arXiv:1505.00404 [astro-ph.CO]].
- [21] L. Xu, Phys. Rev. D **91** (2015), 103520 [arXiv:1410.6977 [astro-ph.CO]].
- [22] V. Pettorino and L. Amendola, Phys. Lett. B **742** (2015), 353-357 [arXiv:1408.2224 [astro-ph.CO]].
- [23] M. Raveri, C. Baccigalupi, A. Silvestri and S. Y. Zhou, Phys. Rev. D **91** (2015) no.6, 061501 [arXiv:1405.7974 [astro-ph.CO]].
- [24] N. Aghanim *et al.* [Planck], Astron. Astrophys. **641** (2020), A6 [arXiv:1807.06209 [astro-ph.CO]].
- [25] P. A. R. Ade *et al.* [BICEP2 and Keck Array], Phys. Rev. Lett. **121** (2018), 221301 [arXiv:1810.05216 [astro-ph.CO]].
- [26] F. Beutler, C. Blake, M. Colless, D. H. Jones, L. Staveley-Smith, L. Campbell, Q. Parker, W. Saunders and F. Watson, Mon. Not. Roy. Astron. Soc. **416** (2011), 3017-3032 [arXiv:1106.3366 [astro-ph.CO]].
- [27] A. J. Ross, L. Samushia, C. Howlett, W. J. Percival, A. Burden and M. Manera, Mon. Not. Roy. Astron. Soc. **449** (2015) no.1, 835-847 [arXiv:1409.3242 [astro-ph.CO]].
- [28] S. Alam *et al.* [BOSS], Mon. Not. Roy. Astron. Soc. **470** (2017) no.3, 2617-2652 [arXiv:1607.03155 [astro-ph.CO]].
- [29] B. P. Abbott *et al.* [LIGO Scientific and Virgo], Phys. Rev. Lett. **118** (2017) no.12, 121101 [arXiv:1612.02029 [gr-qc]].
- [30] B. P. Abbott *et al.* [LIGO Scientific and Virgo], Phys. Rev. D **100** (2019) no.6, 061101 [arXiv:1903.02886 [gr-qc]].
- [31] E. Thrane and J. D. Romano, Phys. Rev. D **88** (2013) no.12, 124032 [arXiv:1310.5300 [astro-ph.IM]].
- [32] C. Caprini, M. Hindmarsh, S. Huber, T. Konstandin, J. Kozaczuk, G. Nardini, J. M. No, A. Petiteau, P. Schwaller and G. Servant, *et al.* JCAP **04** (2016), 001 [arXiv:1512.06239 [astro-ph.CO]].
- [33] R. w. Hellings and G. s. Downs, Astrophys. J. Lett. **265** (1983), L39-L42
- [34] J. P. W. Verbiest, L. Lentati, G. Hobbs, R. van Haasteren, P. B. Demorest, G. H. Janssen, J. B. Wang, G. Desvignes, R. N. Caballero and M. J. Keith, *et al.* Mon. Not. Roy. Astron. Soc. **458** (2016) no.2, 1267-1288 [arXiv:1602.03640 [astro-ph.IM]].
- [35] R. Nan, D. Li, C. Jin, Q. Wang, L. Zhu, W. Zhu, H. Zhang, Y. Yue and L. Qian, Int. J. Mod. Phys. D **20** (2011), 989-1024 [arXiv:1105.3794 [astro-ph.IM]].
- [36] K. Kuroda, W. T. Ni and W. P. Pan, Int. J. Mod. Phys. D **24** (2015) no.14, 1530031 [arXiv:1511.00231 [gr-qc]].
- [37] J. R. Espinosa, D. Racco and A. Riotto, JCAP **09** (2018), 012 [arXiv:1804.07732 [hep-ph]].
- [38] K. Kohri and T. Terada, Phys. Rev. D **97** (2018) no.12, 123532 [arXiv:1804.08577 [gr-qc]].
- [39] K. N. Ananda, C. Clarkson and D. Wands, Phys. Rev. D **75** (2007), 123518 [arXiv:gr-qc/0612013 [gr-qc]].
- [40] C. Armendariz-Picon, V. F. Mukhanov and P. J. Steinhardt, Phys. Rev. D **63** (2001), 103510 [arXiv:astro-ph/0006373 [astro-ph]].
- [41] P. J. Steinhardt and N. Turok, Phys. Rev. D **65** (2002), 126003 [arXiv:hep-th/0111098 [hep-th]].
- [42] D. Battefeld and P. Peter, Phys. Rept. **571** (2015), 1-66 [arXiv:1406.2790 [astro-ph.CO]].
- [43] A. Hojjati, L. Pogosian and G. B. Zhao, JCAP **08** (2011), 005 [arXiv:1106.4543 [astro-ph.CO]].
- [44] A. R. Liddle and D. H. Lyth, Phys. Lett. B **291** (1992), 391-398 [arXiv:astro-ph/9208007 [astro-ph]].
- [45] E. J. Copeland, E. W. Kolb, A. R. Liddle and J. E. Lidsey, Phys. Rev. Lett. **71** (1993), 219-222 [arXiv:hep-ph/9304228 [hep-ph]].
- [46] A. Lewis and S. Bridle, Phys. Rev. D **66** (2002), 103511 [arXiv:astro-ph/0205436 [astro-ph]].
- [47] Y. Akrami *et al.* [Planck], Astron. Astrophys. **641** (2020), A10 [arXiv:1807.06211 [astro-ph.CO]].
- [48] J. Li and Q. G. Huang, Sci. China Phys. Mech. Astron. **62** (2019) no.12, 120412 [arXiv:1906.01336 [astro-ph.CO]].
- [49] A. D. Linde, Phys. Lett. B **129** (1983), 177-181
- [50] A. A. Starobinsky, Phys. Lett. B **91** (1980), 99-102
- [51] G. R. Dvali, Q. Shafi and R. K. Schaefer, Phys. Rev. Lett. **73** (1994), 1886-1889 [arXiv:hep-ph/9406319 [hep-ph]].
- [52] E. J. Copeland, A. R. Liddle, D. H. Lyth, E. D. Stewart and D. Wands, Phys. Rev. D **49** (1994), 6410-6433 [arXiv:astro-ph/9401011 [astro-ph]].
- [53] P. Binetruy and G. R. Dvali, Phys. Lett. B **388** (1996), 241-246 [arXiv:hep-ph/9606342 [hep-ph]].
- [54] E. D. Stewart, Phys. Rev. D **51** (1995), 6847-6853 [arXiv:hep-ph/9405389 [hep-ph]].
- [55] D. H. Lyth and A. Riotto, Phys. Rept. **314** (1999), 1-146 [arXiv:hep-ph/9807278 [hep-ph]].
- [56] R. Kallosh, A. Linde and D. Roest, JHEP **11** (2013), 198 [arXiv:1311.0472 [hep-th]].
- [57] J. Li, Z. C. Chen and Q. G. Huang, Sci. China Phys. Mech. Astron. **62** (2019) no.11, 110421 [arXiv:1907.09794 [astro-ph.CO]].
- [58] J. Li and G. H. Guo, Eur. Phys. J. C **81** (2021) no.7, 602 [arXiv:2101.09949 [astro-ph.CO]].
- [59] J. Li and G. H. Guo, [arXiv:2101.07970 [astro-ph.CO]].
- [60] P. A. R. Ade *et al.* [BICEP/Keck], Phys. Rev. Lett. **127** (2021) no.15, 151301 [arXiv:2110.00483 [astro-ph.CO]].